1

$=1\mathrm{pc}$

Solar Neutrinos at Super-Kamiokande

K.Inoue[a]
for Super-Kamiokande collaboration

[a]Kamioka Observatory, Institute for Cosmic Ray Research, University of Tokyo,
Higashi-Mozumi Kamioka-cho, Yoshiki-gun Gifu 506-12, Japan

A huge ring imaging water Cherenkov detector, super-Kamiokande, has started data accumulation on April 1st, 1996 as promised. This experiment is expected to give a definite answer to the neutrino oscillation solutions of the long standing solar neutrino problem through high statistics and high precision spectrum and day/night flux measurement. Super-Kamiokande is accumulating ^{8}B solar neutrino data very quickly and preliminary results obtained from 374 days of data are presented here, instead of 306 days of data presented at the conference. No significant day/night variation nor seasonal variation are found. Systematic errors of energy scale are largely reduced by the LINAC calibrations at various positions. And the experiment is getting closer to the level of the systematic errors where we can definitely discuss about the spectrum distortion. Also implications of those preliminary results are discussed within two neutrino oscillation hypothesis.

1. Super-Kamiokande

Super-Kamiokande (SK) is a ring imaging water Cherenkov detector located 1,000m (2,700m w.e.) underground in the Kamioka mine in Japan. The detector consists of the 39.3m(ϕ) and 42m(H) main cylindrical tank and 50kton of pure water (currently the water transparency is $\sim$100m at 420nm). Main tank is optically separated to 32.5kton of inner detector viewed by 11,146 50cmϕ PMTs and 2m thickness outer detector viewed by 1885 20cmϕ PMTs. Figure 1 shows a schematic of the detector. Solar neutrino observation uses 22.5kton (2m from the inner wall) as a fiducial volume and rest of the water is used for shielding against gamma rays and neutrons from the surrounding rock (thickness of the shieldings 2.5 to 2.75m) and is also used as an active VETO counter against cosmic ray muons.

SK started taking data in April 1996. However the quality of the water was not very good in April and in May. Actual observation of solar neutrino began in 31th of May with 5.6MeV trigger threshold in an electron total energy. At that time, trigger rate was about 10Hz (3Hz from muons, 7Hz from low energy events). This large detector can provide 13.2 solar neutrino events a day above 6.5MeV (in a total energy of a re-

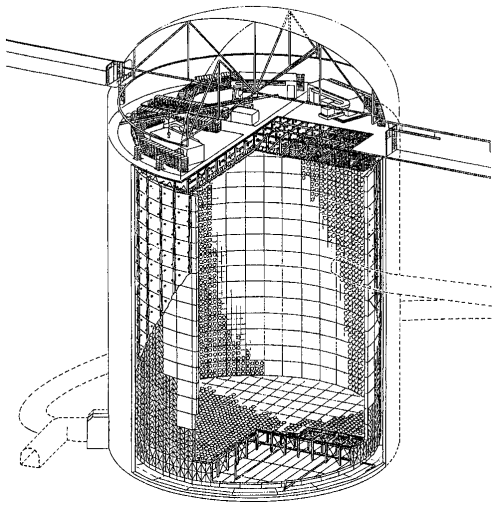

Figure 1. The Super-Kamiokande detector. It contains 50kton of pure water. Inner 32.5kton is viewed by 11,146 50cmϕ PMTs and outer volume viewed by 1885 20cmϕ PMTs is used for an active shielding.

coil electron) in 22.5kton fiducial volume, even after various background rejections. And further challenge to lower the analysis threshold down to 5MeV is being performed since June 1997. An extra super-low-energy trigger (SLE trigger) with 4.6MeV threshold was added with second level reduction on a computer. This SLE trigger causes additional 100Hz in event rate. However most of events have vertices near the wall and by rejecting those wall events with an online program, additional event rate stored in a magnetic tape library is only 5 events/sec. If we succeed to see solar neutrino signal in this super low energy region, not only the statistical precision but also the lever arm to see spectrum distortion will be improved very much.

Because of this high signal rate, SK is expected to examine day/night variation, seasonal variation, spectrum distortion and so on with sufficient sigiframe for testing neutrino oscillation solutions of long standing solar neutrino problem (i.e. large angle solution, small angle solution and Just-so solution).

2. Calibrations

For a discrimination of solar neutrino solutions with any time variations and energy distortions, uniformity of energy scale in direction and in time and also absolute energy scale at various energies are essential and have to be calibrated and be controlled at $\pm 0.5\%$ level. This accuracy requirement is very challenging and will have not been achieved in this kind of large neutrino experiments up to now.

We currently use following 5 different calibration sources.

1. spallation products by cosmic ray muons
2. gamma rays from neutron absorption on Ni
3. decay electron from stopped muon
4. ^{16}N from muon absorption on oxygen
5. electrons from a linear accelerator (LINAC)

Best qualities of calibrations are obtained from spallation and LINAC, and the others are giving supplement calibrations, currently.

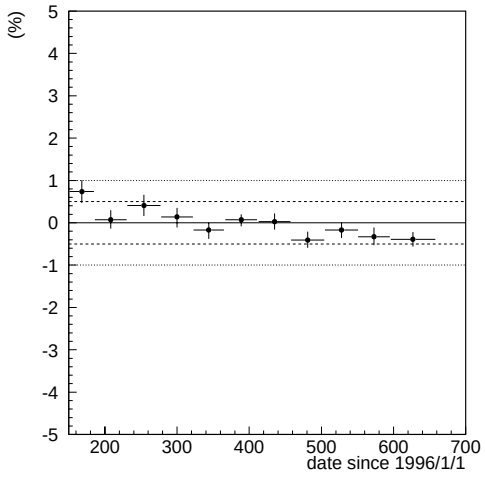

Figure 2. Stability of the detector in time. The relative energy scale change obtained from spallation events is shown as a function of time. Solid line, dashes and dots show 0%, $\pm 0.5\%$ and $\pm 1.0\%$ respectively.

Spallation events are accumulated in the data as a major background, however, their average beta decay spectrum is similar to ^{8}B spectrum, also they are distributing uniformly in volume, in direction and in time as are solar neutrinos. Thus, the major background is a good calibration source. Figure 2 and figure 3 show the stability of relative energy scale in time and the relative energy scale as a function of radius using those spallation events, respectively. Both calibrations resulted better than $\pm 0.5\%$ uniformities.

The most important progress was carried out from the LINAC calibrations. LINAC is placed in the sub-access-tunnel to the top of the detector and can emit electrons with energies upto 17MeV which covers the energy region interested in solar neutrino observation. Electron energies are calibrated by a germanium detector with better than 20keV accuracy. And electrons have been injected downward to SK tank with seven different energies and at six different positions. The accuracy

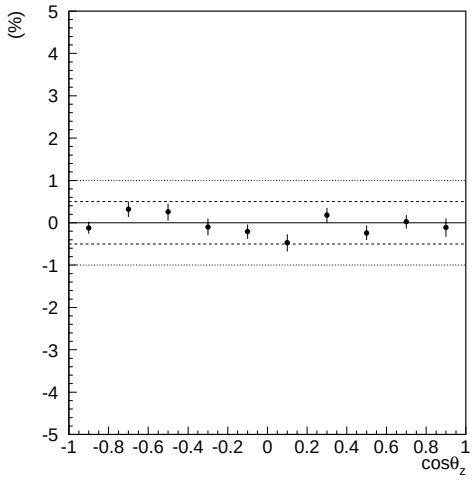

Figure 3. Uniformity of energy scale in direction. The relative energy scale obtained from spallation events is shown as a function of cosine of nadir. Solid lines, dashes and dots are the same as figure 2.

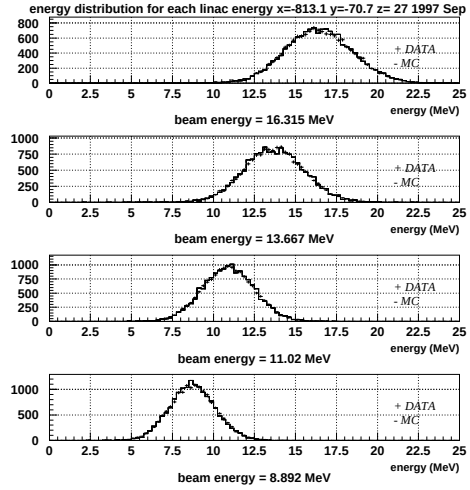

Figure 4. Energy distributions of the linac calibration. Denoted beam energies are the electron total energies in the beam pipe. Horizontal axis is a reconstructed total energy by SK.

of visible energies in the SK tank is estimated to be $\pm 0.6\%$ at 6MeV and $\pm 0.3\%$ at 10MeV considering reflection of Cherenkov photons on the LINAC beam pipe and so on. This very accurate beam is an essence of the calibration of absolute energy scale. And a well-collimated electron beam also provided precise calibration of an angular resolution which plays important rôle at an extraction of directional solar neutrino events against uniform background. Typical energy distributions and direction distributions are shown in figure 4 and in figure 5, respectively, together with the expectation from a tuned MC. The MC reproduces energy and direction distributions very well as shown in figure 6 and in figure 7. The energy dependence of the difference is less than $\pm 0.3\%$ for energies above the analysis threshold (6.5MeV) and the position dependence leads $\pm 0.3\%$ systematic error in an extrapolation of the energy scale determined at 6 positions to the entire fiducial volume.

In an early stage of SK experiment, we didn't have the LINAC and we used Ni gamma rays for the calibration of an absolute energy scale. After the accurate LINAC calibrations, we found that the scale obtained by Ni gives +2.2% higher energies than that obtained by the LINAC. This difference has been investigated. And our current knowledge is as follows. (a) -0.8% gamma ray contamination from surrounding materials (hanging wire, bolts and nuts, signal cables, container of fission source and so on). This contamination was measured by replacing target Ni with H_3BO_3 which has large cross section of $^{10}B(n,\alpha)^7Li$ with the same amount of neutron absorption cross section. (b) $-0.25\% \pm 0.25\%$ obstacle around Ni containers. We simulated wires, cables and so on as detail as possible, and found 0.5% of Cherenkov photon hits those obstacle. However we don't know reflectance and put $50\% \pm 50\%$ for it. (c) $-0.2\% \pm 0.2\%$ position dependence of neutron capture. We didn't trace behavior of neutrons from fission source upto capture on nickel

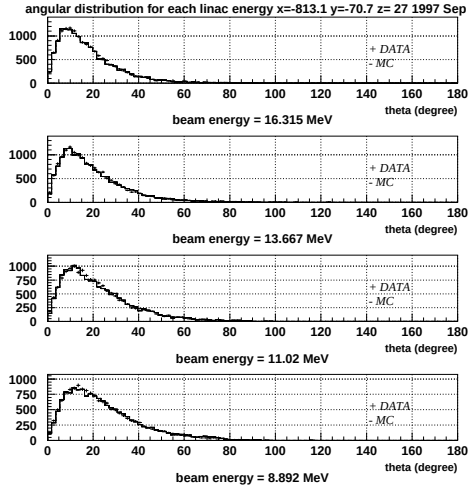

Figure 5. Direction distributions of the linac calibration with respect to the injected direction.

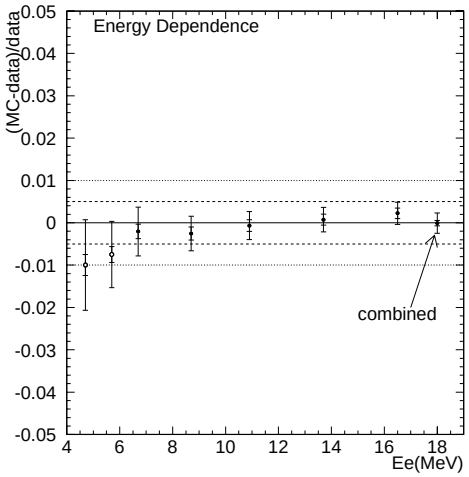

Figure 6. Energy dependence of the MC tuning. Each point shows an averaged value over 6 different positions. Inner error bars are statistical and outer bars are systematic errors added in quadrature. The combined point is an average of 5 different energies shown as black circles. Horizontal axis is a reconstructed total energy.

in a simulation. That will cause mismatch of the generated position distribution of gamma rays. Then, the attenuation of gamma rays in material may not be simulated correctly. (d) +0.15%: absorption on ^{64}Ni. We neglected small absorption probability of neutrons on ^{64}Ni. (e) ±0.5% lines in ^{60}Ni and ^{62}Ni. We didn't simulate very detail of decay lines of ^{60}Ni and ^{62}Ni. (f) ±0.5% uncertainty of capture cross sections.

As a result, we found +1.4%±0.8% error in our previous Ni-based energy scale. By correcting it, the difference between Ni and LINAC is 0.8%±0.8% and both calibrations are more or less consistent. And, we see the Ni source does not match for the calibration of the absolute energy scale at ±0.5% level.

3. Reductions

The solar neutrino data used in this report covers a period from 31th of May 1996 through 20th of Oct 1997, and the total live time is 374.2 days out of 508 days calendar time. Most of the dead time comes from calibrations and preparation for them. Total number of triggered events is about 400 million. Then, we reject muons, noise events (electronics noise, flashing PMT etc), decay electrons from stopped muons and so on. Then, we set 22.5kton fiducial volume (2m from the inner wall) and the event rate above 6.5MeV is 0.016Hz at this step. Most of the events near the wall are thought to be gamma rays from materials and rocks around the detector. Figure 8 shows energy spectrum of (△) after fiducial cut together with the other steps (◇) after spallation cut, (◯) after gamma cut, (−) expected ^{8}B neutrino events from BP95[1] and (•) observed solar neutrino events.

Now, the dominant background are the spallation products made by cosmic ray muons. They are beta emitters with mass number less than 16. Since energetic muons cause those spallations and lifetimes of the beta emitters are less than

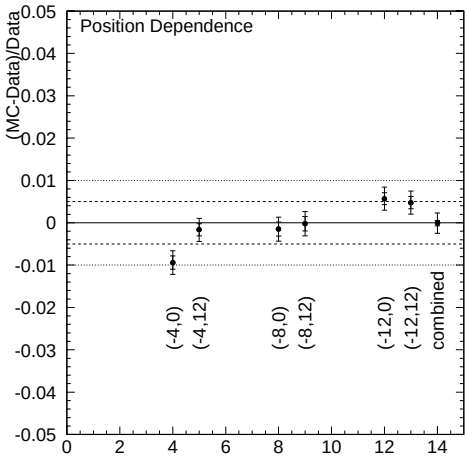

Figure 7. Position dependence of the MC tuning. Each point shows an averaged value over 5 different energies above 6.5MeV. Error bars are same as figure 6. Injected positions are labeled below data points as (x,z) in meter.

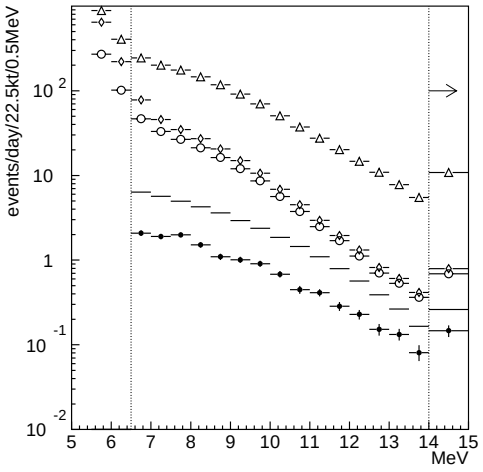

Figure 8. Energy spectra of (△) after fiducial cut, (◇) after spallation cut, (◯) after gamma cut, (−) expectation from B8 and (●) observed solar neutrino events. The last points are integrated from 14MeV to 20MeV.

a minute (typically 10msec), we can reject those events by looking at correlations of muons and low energy events in space (ΔL) and in time (ΔT) and by looking at extra energy deposit of muons associating cascade (ΔE). We developed a likelihood function with those measures, ΔT, ΔL and ΔE. By maximizing $S/\sqrt{N}$, we obtained reduction factor 6 with 20.0% inefficiency in the spallation cut. The event rate is, then, 2.9×10^{-3}Hz.

Direction and vertex distributions after the spallation cut is shown in figure 9. As seen in the figure, there is a large background toward the wall even in the fiducial volume and those events make direction distributions very wavy. In order to remove those events, we defined an effective distance from the wall (distance along the event direction) and set 4.5m as an minimum value. That gamma cut reduces 30% of events with 8.0% inefficiency for solar neutrino events. The beauty of the gamma cut is a resultant uniform direction distribution as seen in figure 9. This uniformity makes a systematic bias minimum when we extract solar neutrino signals with direction information. Here, we have obtained final sample, and number of events is 6550 or the final event rate is 2.03×10^{-3}Hz from 6.5 to 20MeV.

Signal extraction is done by fitting angular distributions toward the sun with the angular resolution function obtained by the LINAC calibration and the non-flat background shape estimated from the $\cos\theta_z$ distribution of the data itself (thus, it is almost flat due to the gamma cut). Figure 10 shows the best fit of the angular distribution for the events above 6.5 MeV and in 22.5kton fiducial volume. In this fit, number of solar neutrino events is obtained as $4651.8^{+117.9}_{-111.3}$ for 374.2 days of data. This is quite large value in comparison with the Kamiokande result[2] 597^{+41}_{-40} for 2079 days of data.

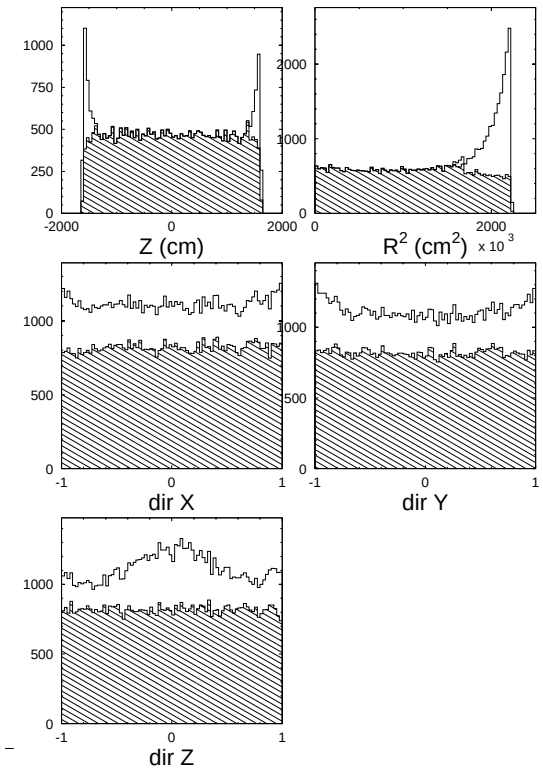

Figure 9. Vertex and direction distributions before and after the gamma cut. The final sample is after the gamma cut (hatched).

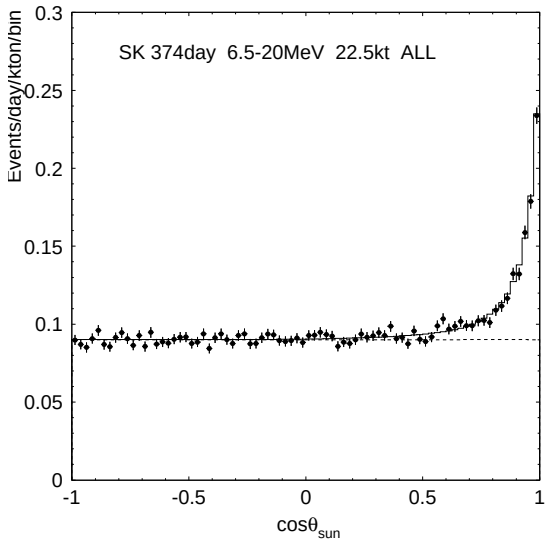

Figure 10. Angular distibution toward the sun. Events used here are energies from 6.5 to 20MeV and verticies in 22.5kton fiducial volumn. Plots are the data and histogram is the best fit assuming ^{8}B neutrino spectrum. Dashed histogram is an expected non-flat background distribution.

4. Solar ν results

Figure 11 shows neutrino oligraph taken by SK. Events used in the picture are the final sample (6.5-20MeV in 22.5kton of 374.2days during May 31,1996 through Oct 20,1997). Using these solar neutrino events, we have obtained preliminary results of ^{8}B solar neutrino flux, seasonal and day/night variations and energy spectrum as follows.

The ^{8}B solar neutrino flux is (here we assume a spectrum given by Bahcal[3]);

$$\phi_{^8B} = 2.37^{+0.06}_{-0.05}(stat.)^{+0.09}_{-0.07}(syst.)[\times 10^6/cm^2/sec]$$

or by taking ratio to the BP95[1] flux, we obtain;

$$\frac{Data}{SSM_{BP95}} = 0.358^{+0.009}_{-0.008}(stat.)^{+0.014}_{-0.010}(syst.)$$

And the flux difference between day and night is;

$$\frac{D-N}{D+N} = -0.031 \pm 0.024(stat.) \pm 0.014(syst.)$$

And, night data is further divided into 5 bins as shown in figure 12. We don't see very significant difference in day/night fluxes. In the figure, the expected day/night variations of the typical large angle ($sin^2 2\theta = 0.66, \Delta m^2 = 2.82 \times 10^{-5}$) and the typical small angle ($9.12 \times 10^{-3}, 6.31 \times 10^{-6}$) solutions are overlaid.

The seasonal variation is investigated by dividing data into 8 periods as shown in figure 13. In the figure, expected flux variation from the eccentricity of the earth's orbit around the sun is also shown as a solid line. We don't see any signifi-

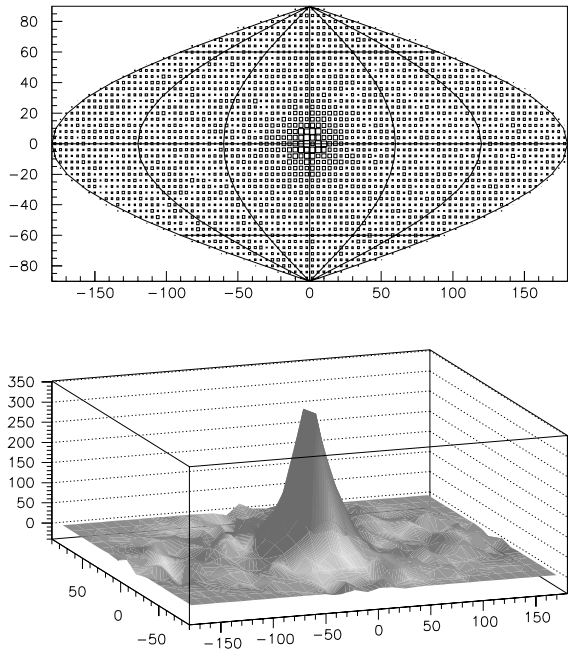

Figure 11. The neutrino heliograph. Size of the boxes shows an intensity in the upper figure and the sun is located at the center. In the lower figure, intensity is a height and background is subtracted.

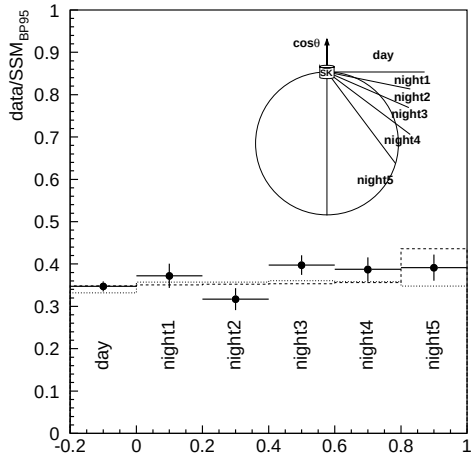

Figure 12. Day/Night variation. Error bars are statistical only. Night data is divided into 5 bins. Night 1 is horizontal direction and night 5 is vertical direction (neutrino comes from the other side of the earth). Dotted histogram is the expected variation of the typical large angle solution and dashed histogram is that of the typical small angle solution.

cant seasonal variation and the statistics is still insufficient to observe eccentricity curve, yet.

The energy spectrum is shown in figure 14. Systematic errors have been reduced very much due to the LINAC calibrations. In the figure, expected spectrum of the typical small angle $(9.12 \times 10^{-3}, 6.31 \times 10^{-6})$ and the typical just so $(0.83, 7.08 \times 10^{-11})$ solutions are overlaid. It is hard to say spectrum distortion from this figure. But, small angle solution gives better fit than a flat spectrum (no oscillation) and just so solution gives slightly better fit than the small angle solution. However, they are not yet significant as discussed in the next section.

Systematic errors of the energy scale can make distortion in energy spectrum, and it may fake the neutrino oscillation signature. Therefore, systematic errors are investigated extensively especially for the energy scale. As written in the section on "Calibrations", the LINAC improved intrinsic scale error very much. However, we have to consider following errors as the scale error (errors which cause spectrum distortion) in translation of the LINAC data to the detector systematic error. LINAC data have been taken at 7 different but fixed energies, 6 different but fixed positions and also the beam is injected only downward. We use MC for extrapolating these calibrations so entire energies, volume and direction. So, some errors listed are coming from the reproducibility of our

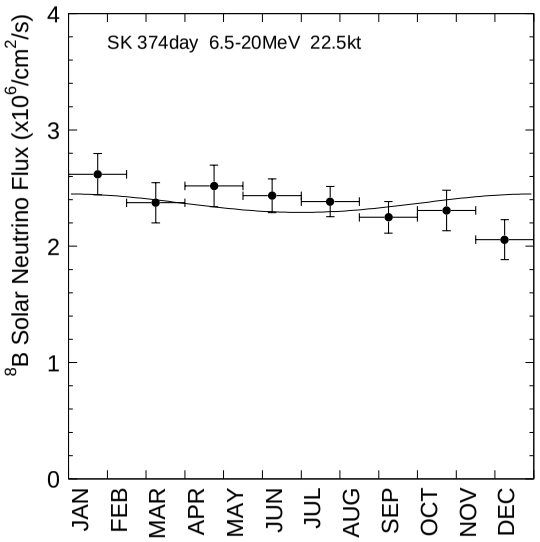

Figure 13. Seasonal variation. Each season is piledup among different years. Solid lineshows the expected variationfrom an eccentricity of the orbit.

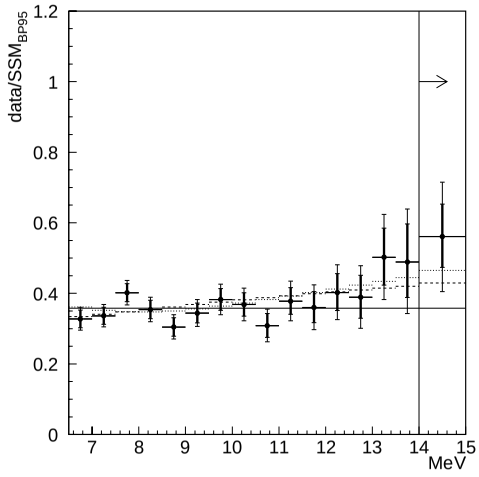

Figure 14. Energy spectrum. Inner error bars are the statisticalones and outer bars are the systematic errorsadded linearlywith statisticalones. Dashed histogram isthe expected spectrum of the typical small angle solutionand dotted histogram isthat of the typical justso solution.

MC.

1. LINAC intrinsicerror: It is energy dependent and typically 0.6% at 6MeV and 0.3% at 10MeV.
2. MC tuning precision: 0.1%
3. difference of position dependence between data and MC: 0.3%
4. precision of transparency measurement at the LINAC calibration: 0.2%
5. difference of direction dependence: 0.5% This is obtained from spallation events.
6. energy dependent scale difference between data and MC: 0.3% at 6MeV, 0.1% at 10MeV

By combining these errors, we obtain energy dependent scale errors and the values are typically 0.9% at 6MeV and 0.7% at 10MeV. These values are a littleworse than the value 0.5% which we set as a goal. In order to reach at 0.5% accurate energy calibrations in different directions is needed. In addition to this scale eror, misunderstanding of energy resolution and an uncertainty of ^{8}B spectrum itselfcan distort energy spectrum. Our MC can reproduce measured energy resolution within 2%. These experimental errors reflect to the systematic error in flux as $^{+1.3}_{-1.3}$% at 6.5-7.0MeV, $^{+2.0}_{-2.0}$% at 9.0-9.5MeV, $^{+4.1}_{-4.6}$% at 11.5-12.0MeV and $^{+8.5}_{-11.0}$% at 14.0-20.0MeV. And the ^{8}B spectrum error by Bahcall[3] at 3σ level. We took one third of the error as a systematic error. The systematic error coming from this shape error is energy dependent and typical values are $^{+0.5}_{-0.1}$% at 6.5-7.0MeV, $^{+1.4}_{-1.3}$% at 9.0-9.5MeV, $^{+3.2}_{-2.7}$% at 11.5-12.0MeV and $^{+6.9}_{-4.9}$% at 14.0-20.0MeV. This error is rather large and it will soon become dominant by an improvement of the experimental errors. All the above errors are combined in table 1. This energy dependent

Table 1
Systematic errors. Errors are shown in %. Flux error is an absolute systematic error but the others are relative errors. And errors coming from "Energy scale & resolution" and "^{8}B spectrum" are correlated errors in spectrum analysis.

	Flux	Seasonal	D/N	Spectrum
Energy scale & resolution	$+2.3 - 2.1$	$+1.2 - 1.1$	$+1.2 - 1.1$	$^{+1.4}_{-1.3}@^{6.5-}_{7.0MeV}$ $^{+2.5}_{-2.4}@^{9.0-}_{9.5MeV}$
^{8}B spectrum	$+1.2 - 1.1$	–	–	$^{+5.2}_{-5.3}@^{11.5-}_{12.0MeV}$ $^{+11.0}_{-12.1}@^{14.0-}_{20.0MeV}$
Trigger efficiency	$^{+0.2}_{-}$	$^{+0.2}_{-}$	–	$^{+1.2}_{-}@^{6.5-}_{7.0MeV}$
Noise event cut	± 0.7	–	–	± 0.7
Direction resolution	$^{+2.9}_{-}$	–	–	± 1.0
Reduction efficiency	± 0.2	–	± 0.1	± 0.2
non-flat B.G.	± 0.1	± 0.1	± 0.4	± 0.1
Spallation dead time	< 0.1	± 0.6	± 0.6	–
Vertex shift	-1.3	–	–	± 1.0
Cross section	± 0.5	–	–	± 0.5
Live time	± 0.1	± 0.1	± 0.1	–
Total	$^{+4.0}_{-2.9}$	$^{+1.4}_{-1.3}$	$^{+1.4}_{-1.3}$	see figure 14

spectrum error is fully correlated among energy bins. All the breakdown of systematic errors are also shown in the same table.

5. Implications in neutrino oscillation

Impact of the preliminary results from 374 days data was investigated within $\nu_e \rightarrow \mu_{\mu,\tau}$ oscillation hypothesis. Oscillational calculations have been done both for MSW [5] parameter region ($10^{-4} < \sin^2 2\theta < 1, 10^{-8} < \Delta m^2 < 10^{-3} eV^2$) and for Just-so [6] parameter region ($0 < \sin^2 2\theta < 1, 10^{-11.25} < \Delta m^2 < 10^{-9.25} eV^2$).

Since the ^{8}B solar neutrino flux has a large uncertainty ($6.62 \times (1.00^{+0.14}_{-0.17}) \times 10^6 / cm^2/sec$ [1]). We first performed a flux independent analysis on the D/N variation and on the spectrum distortion. We defined follwing χ^2 and the flux normalization factor α was treated as a free parameter.

$$\chi^2_{D/N} = \sum_{i=D,N1,\cdots,N5} \left\{ \frac{\left(\frac{Data}{SSM}\right)_i - \alpha \times R_i^{osci}}{\sqrt{\sigma_i^2 + \sigma_{sys}^2}} \right\}^2$$

where Data/SSM is the results shown in figure 12, R_i^{osci} the ratio of expected event rate with oscillation to that without oscillation for each $(\sin^2 2\theta, \Delta m^2)$, σ_i the statistical error of i-bin and σ_{sys} the systematic error listed in table 1.

$$\chi^2_{spec} = \sum_{i=1,16} \left\{ \frac{\left(\frac{Data}{SSM}\right)_i - \alpha \cdot R_i^{osci} \cdot f(\beta)}{\sqrt{\sigma_i^2 + \sigma_{un.sys}^2}} \right\}^2 + \left(\frac{\beta}{\sigma_\beta}\right)^2$$

where Data/SSM is the results shown in figure 14, $f(\beta)$ the response function of the correlated errors in table 1, β the parameter that controls a slope of energy spectrum through the function f and σ_{unsys} the uncorrelated systematic error combined in quadrature. By using these χ^2, we looked for the minimum in each MSW and Just so region, independently The contour maps shown in figure 15 and in figure 16 are the equal-distant (5.99 for 95% and 9.21 for 99% C.L.) lines from χ^2_{min}. And in those figures, also shown as shaded are the allowed region obtained by Hata and Langacker [4] considering all the solar neutrino experiments. D/N analysis gave $\chi^2_{min} = 4.1$ at $(1.26 \times 10^{-2}, 3.98 \times 10^{-6})$ near the small angle solution at 5 degree of freedom and excluded a half of the large angle solution. Because of a good fit of spectrum in Just so region, flat (no oscillation) is excluded at 95% C.L. It is not significant very much, and flat revives at 99% C.L. However, it is

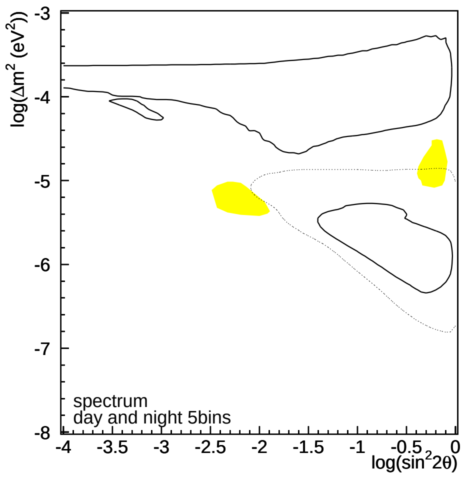

Figure 15. 95% C.L. excluded region at MSW region. D/N analysis excludes dotted region and spectrum analysis excludes regions inside of solid lines. Shaded region is the 95% C.L. allowed region by Hata and Langacker [4].

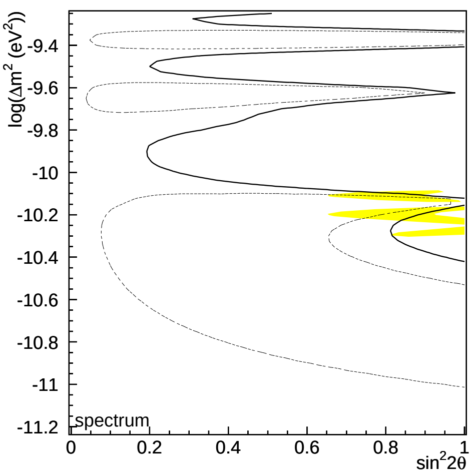

Figure 16. 95% C.L. and 99% C.L. contour at Just so region. Inside of dotted line is excluded at 95% C.L. and inside of solid line is excluded at 99% C.L. from spectrum analysis.

quite encouraging in the sense that we are almost reaching at the level of statistics and systematics where we can discuss about the spectrum distortion.

Then, we performed a flux constrained analysis with the following χ^2.

$$\chi^2_{tot} = \sum_{\substack{i=D,N\\ j=1,16}} \left\{ \frac{\left(\frac{Data}{SSM}\right)_{ij} - \alpha \cdot R^{osci}_{ij} \cdot f(\beta)}{\sqrt{\sigma^2_{ij} + \sigma^2_{un.sys}}} \right\}^2 + \left(\frac{1-\alpha}{\sigma_\alpha}\right)^2 + \left(\frac{\beta}{\sigma_\beta}\right)^2$$

where σ_α is the flux error $^{+0.14}_{-0.17}$ given by Bahcall [1]. χ^2_{min} was looked for both in MSW and in Just so regions, simultaneously in this case. The minimum was found at $(\sin^2 2\theta, \Delta m^2) = (0.562, 1.41 \times 10^{-7} eV^2)$ and the value was 39.5 with 32 degree of freedom. The χ^2 values at "typical" small angle, large angle and just so solution parameters were 40.8 $(9.12 \times 10^{-3}, 6.31 \times 10^{-6})$, 41.6 $(0.66, 2.82 \times 10^{-5})$ and 40.4 $(0.83, 7.08 \times 10^{-11})$, respectively. Three solutions have similar probability in the preliminary results. Figure 17 and figure 18 show equal-confidence-level contours at 68%, 90% and 95%. All three solutions obtained by Hata and Langacker [4] still overlap with the allowed region obtained here. Expected spectra and day/night variation at the above three "typical" parameters are overlaid with the SK results in figure 12 and in figure 14. Looking at those spectra and day/night variations at typical parameters, we expect (1) spectrum distortion and night excess for small angle solution, (2) uniform increase of night fluxes for large angle solution and (3) spectrum distortion and no night excess for just so solution. That means each solution has each different signature of neutrino oscillation. And we expect that SK

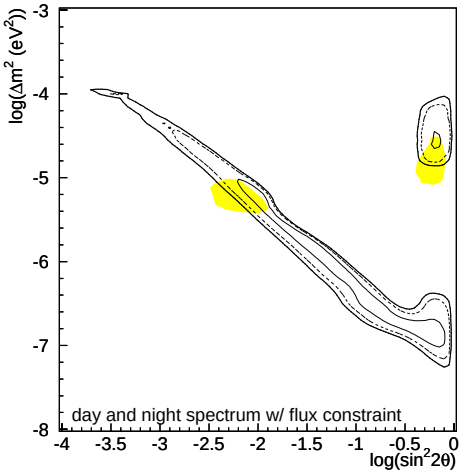

Figure 17. The 95% (thick solid), 90% (dashed) 68% (thin solid) C. L. allowed region from D/N and spectrum combined analysis with flux constraint are shown. Shaded region is the allowed region by Hata and Langacker [4].

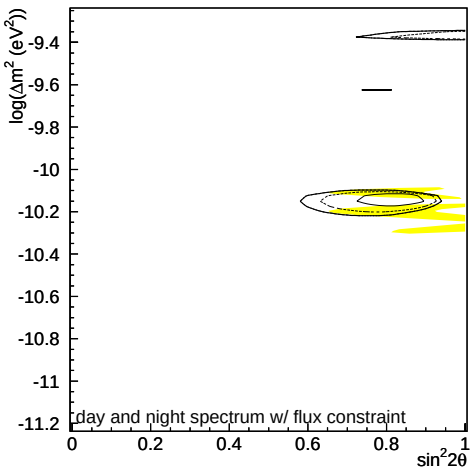

Figure 18. Same as figure 17 at Just so region.

will definitely discriminate those three solutions in a few years. And for just so solution, we may see a peculiar seasonal variation as a supplemental evidence sevral years later.

6. Summary

The statistics of solar neutrino events is increasing very quickly. And also the systematic errors were reduced drastically by the LINAC calibration. The preliminary solar neutrino results from SK 374 days were reported with such high statistics and small systematics. The obtained ^{8}B solar neutrino flux is apparently smaller than the expectation from the standard solar model. However, SK doesn't show very significant time variations nor spectrum distortion yet. And the data still allows all three solar neutrino solutions (i.e. small angle, large angle and just so solutions) at almost same probabilities. But, it is certain that we are almost reaching at the level of statistics and systematics where we can definitely discuss about neutrino oscillation solutions and SK has a capability to distinguish neutrino oscillation solutions. Let's look forward to see definite answer appears in a few years.

REFERENCES

1. J. N. Bahcall and M. H. Pinsonneault Rev. Mod. Phys. 67, 781 (1995).
2. Y. Fukuda et al., Phys. Rev. Lett. 77, 1683 (1996).
3. J. N. Bahcall et al., Phys. Rev. C54, 411 (1996).
4. N. Hata and P. Langacker, IASSNS-AST 97/29, UPR-751T, hep-ph/9705339, May 1997.
5. L. Wolfenstein Phys. Rev. D17, 2369 (1978), D20, 2634 (1979),
   S. P. Mikheyev and A. Yu. Smirnov Sov. J. Nucl. Phys. 42, 913 (1985).
6. L. Glashow and L. M. Krauss Phys. Lett. B190, 199 (1987).